Decoding ECoG High Gamma Power from Cellular Calcium Response using Transparent Graphene Microelectrodes

Xin Liu, Chi Ren, Yichen Lu, Ryoma Hattori, Yuhan Shi, Ruoyu Zhao, David Ding, Takaki Komiyama, and Duygu Kuzum

Abstract—The ECoG has been widely used in human brain research, while 2-photon microscopy has been broadly applied to basic neuroscience studies using animal models. Bridging the gap between the 2-photon microscopy and the ECoG is critical for transferring the vast amount of neuroscience knowledge obtained from animal models to human brain studies. Here we develop an LSTM recurrent neural network model to decode the ECoG high gamma power from the cellular calcium activities obtained by multimodal ECoG recordings and 2-photon calcium imaging enabled by transparent graphene microelectrode arrays. In both awake and anesthetized states, our model can successfully decode the stimulus-induced ECoG high gamma power increases and its spontaneous fluctuations in the absence of stimulus.

I. INTRODUCTION

Electrocorticography (ECoG) has been widely used in basic neuroscience research to investigate neural activities across large brain areas, as well as clinical settings to provide real-time brain monitoring in human patients with epilepsy. For example, using ECoG recordings, it has been discovered that cortical traveling waves may play important roles for memory formation [1]. ECoG has also been used to improve the performance of brain-computer interfaces by providing higher spatial resolution than the conventional EEG-based approaches [2-4]. It has been recently shown that ECoG recordings can be used to decode human moods [5]. On the other hand, large amounts of neuroscience research performed in animal models uses 2-photon microscopy [6, 7], providing much finer spatial resolution and capability of recording from hundreds of neurons with limited temporal resolution. In order to transfer the knowledge obtained in animal studies to human brain research, the gap between these two methodologies needs to be closed. Therefore, as a first step forward, it is important to build a model that can decode the observed ECoG potentials from cellular calcium activities. To develop an accurate model, multimodal experiments combining ECoG recordings with 2-photon microscopy are needed to be performed.

Here, using a transparent graphene microelectrode array, we perform multimodal electrophysiological recordings and 2-photon calcium imaging to obtain the simultaneous ECoG

signals and the underlying cellular activities. Then, we train a long short-term memory (LSTM) recurrent neural network model using simultaneously recorded ECoG potentials and calcium fluorescence response from individual neurons. The recurrent neural network trained using multimodal data is used to decode ECoG from calcium imaging data. In this work, we employ our model to decode stimulus-related ECoG high gamma power increases and the slow-oscillation modulated rhythmic high gamma power changes for the anesthetized state. In addition, our model successfully decodes stimulus-induced ECoG high gamma power and irregular spontaneous ECoG power fluctuations between two stimuli in the awake state.

II. METHODS

A. Fabrication Process of the Transparent Graphene Array

Graphene microelectrode array was fabricated following the procedures reported in our previous studies [8, 9]. Figure 1a shows a picture of the 16-channel graphene array. In this study, we chronically implanted the array over mouse visual cortex for over 20 days. The array impedance remains stable for over 20 days after implantation (Figure 1b). Figure 1c is a schematic of the experimental setup for simultaneous electrical recording and 2-photon calcium imaging.

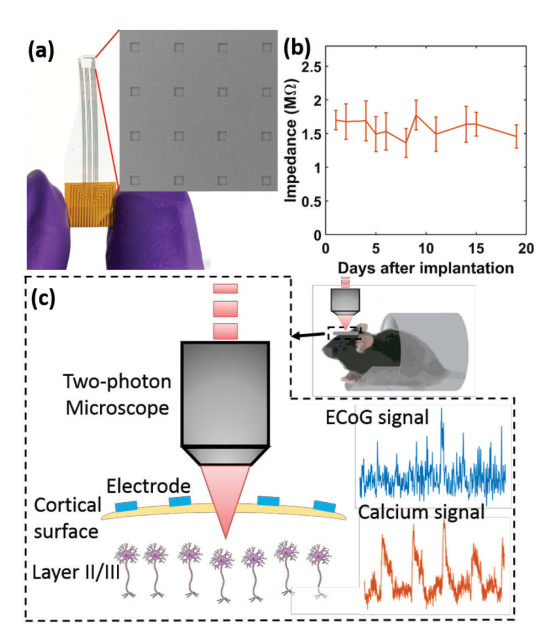


Figure 1. The graphene array and the recording setup. (a) A picture of the graphene microelectrode array. (b) Impedance of the array as a function of days after implantation. (c) A schematic showing simultaneous 2-photon calcium imaging and electrical recording setup.

^{*} This research was supported by the Office of Naval Research (N000141612531) and the National Science Foundation (ECCS-1752241, ECCS-1734940).

X. Liu, Y. Lu, Y. Shi, R. Zhao, D. Ding, and D. Kuzum are with the Department of Electrical and Computer Engineering, University of California San Diego, CA, 92093, USA (e-mail: xil432@eng.ucsd.edu).

C. Ren, R. Hattori, and T. Komiyama are with the Neurobiology Section and Department of Neurosciences, University of California San Diego, CA, 92093, USA.

B. Animal Experiment Procedures

Adult mice (cross between CaMKIIa-tTA (JAX 003010) and tetO-GCaMP6s (JAX 024742), 2 months old) were anesthetized with isoflurane (3% for induction and 1% for maintenance) and a circular piece of scalp was removed. A custom-built head-post was implanted to the exposed skull (1 mm posterior to lambda) with cyanoacrylate glue and cemented with dental acrylic (Lang Dental). A stainless-steel screw (F000CE156, J.I. Morris) was implanted over right olfactory bulb as reference. A square craniotomy (4 x 4 mm) was made over the left hemisphere and the graphene microelectrode array was implanted to cover visual cortices. A glass imaging-window was placed on top of the electrode array and further secured with vetbond (3M) and dental acrylic. For anesthesia experiments, mice were anesthetized by intraperitoneal injections of ketamine/xylazine (100 mg/kg and 8 mg/kg, respectively). A custom 3D-printed case was employed to protect the electrode array when mice were in home cage.

C. Visual Stimulus and Imaging Setup

Square-wave drifting grating stimuli (100% contrast, 0.04 cycles/degree, 3 cycles/sec, covering entire contralateral receptive field) were presented on a LCD monitor (30 × 38 cm) positioned 15 cm away from the right eye using Psychtoolbox (http://psychtoolbox.org/). One of 12 orientations (30° apart) was presented for 4 sec on each trial in pseudorandom order. Inter-stimulus-interval was varied between 7-9 seconds. We presented each orientation at least 10 times in a session.

2-photon calcium imaging was conducted for a head-fixed mouse using a 925 nm laser (Ti:sapphire laser, Newport) through a 16×0.8 NA objective (Nikon) mounted on a commercial 2-photon microscope (B-scope, Thorlabs). Images were acquired at ~29 Hz with a resolution of 512×512 pixels, covering $786 \times 846 \ \mu m^2$. Acquired images were motion corrected offline. Fluorescence from cell bodies was extracted using Suite2P [10]. We applied non-negative deconvolution to the cellular fluorescence to estimate the spiking activities [11].

III. RESULTS

A. Simultaneous ECoG and Calcium Imaging

As shown in Figure 2a, the imaging window stayed clear for many days after the implantation and we were able to obtain high quality calcium fluorescence response data recorded from different areas of the mouse cortex with simultaneous electrical recordings. Figure 2b shows some representative 2-photon microscope images taken at 250 µm depth, corresponding to the Layer II/III of the visual cortex. The neurons were clearly identifiable through the transparent graphene array. As shown in Figure 2c, under the awake state, there was obvious and stable stimulus-induced visual responses indicated by an increase of the mean cellular fluorescence levels in the imaging region of interest (ROI). In awake state the spiking activities were in general elevated due to the visual stimulus, but remained sparse and stochastic (see the black traces in Figure 2c). On the other hand, under anesthetized state, the mean cellular fluorescence signals exhibited obvious 1-2 Hz fluctuations (The blue traces in Figure 2c), which is due to the 1-2 Hz slow oscillations commonly observed during anesthesia, modulating the firing activities of individual neurons [12, 13].

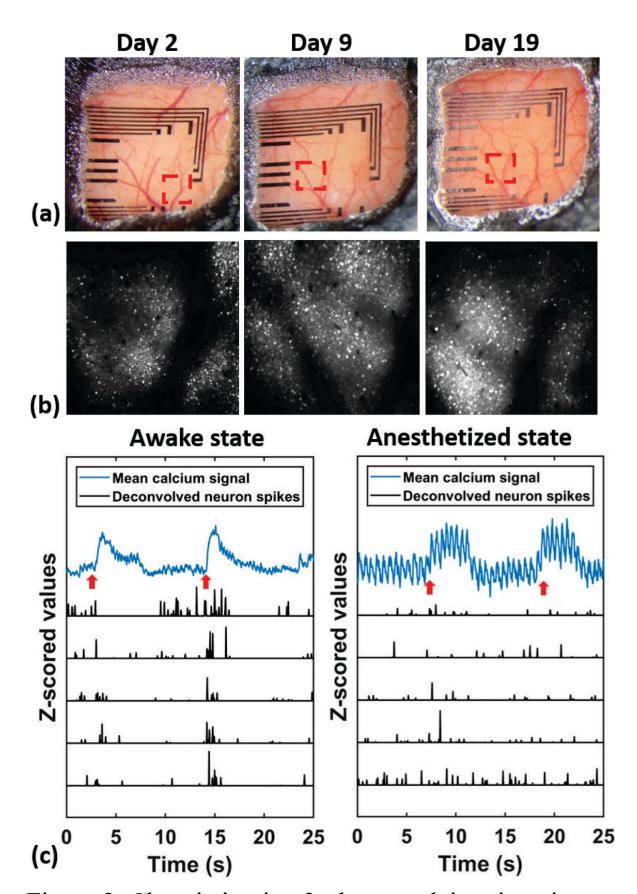


Figure 2. Chronic in vivo 2-photon calcium imaging. (a) Pictures of the imaging window at different days after the implantation, showing the mouse cortex and the graphene array. (b) Images taken by the 2-photon microscope at 250 µm depth under the red outlined area. (c) Representative calcium responses taken at 250 µm depth for the awake (left panel) and anesthetized states (right panel). The red arrows indicate the arrival times of the visual stimulus. The blue line shows the z-scored mean cellular fluorescence signal. The black traces are some representative z-scored spiking activities from different neurons.

In the ECoG recordings, we also observed consistent and reliable visual responses. Figure 3a shows the trial averaged ECoG on-response recorded in all the 16 channels when the stimulus is arrived. It can be seen that this on-response is phase-locked to the stimulus time in both the awake and anesthetized state. Besides this stimulus induced time- and phase-locked on-response, we also observed high gamma range (60–200 Hz) ECoG power increases, consistent with the recordings in literature [14]. Figure 3b shows the trial-averaged time frequency power difference D(w,t)around the onset time of the visual stimulus for both awake and anesthetized states. The formula for obtaining this plot is shown in equation (1), which has been used in the previous studies on visual response [14]. S(w,t) is the trial-averaged power between [-1, 8] seconds around the stimulus time and B(w,t) is the averaged baseline power during 1 second before the visual stimulus. Since there is a 1/f power decay in the neural signals, responses in the high frequency power ranges can be hard to visualize [15]. By performing the transformation shown in equation (1), instead of looking at the absolute power magnitude, we are focusing on the power increase ratio at individual frequencies compared with the baseline power magnitude. It can be seen that when the visual stimulus comes, there is significant power increase in the high gamma frequency band. Unlike the transient on-response, the elevation of high gamma power sustains during the presence of ~4s visual stimulus. Note that the power increase ratio during the anesthetized state is larger than that during the awake state. This is because the baseline high gamma power in the awake state is higher than that during the anesthetized states, leading to a smaller power increase ratio.

$$D(w,t) = 10 \cdot (\log_{10} S(w,t) - \log_{10} B(w,t)) \tag{1}$$

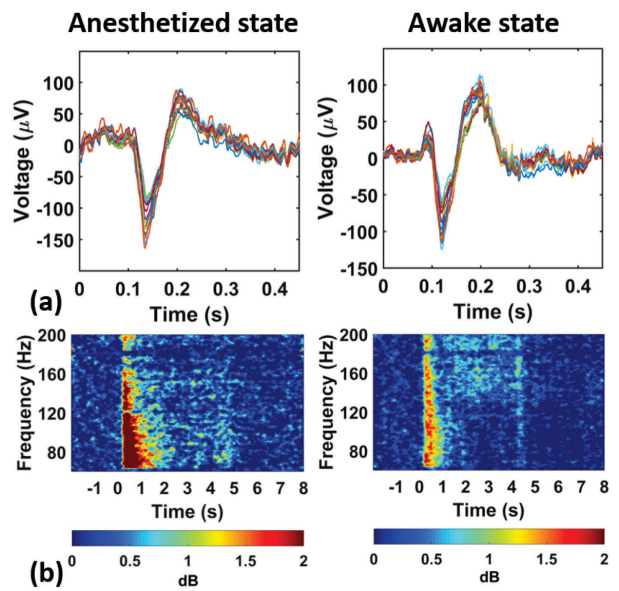


Figure 3. ECoG visual responses under anesthesia and awake states. (a) The averaged ECoG signals showing the on-response right after the onset of visual stimulus (time = 0s). Different colors represent the electrical signals from all the 16 channels. (b) Normalized average spectrogram D(w,t) showing the high gamma band (60-200 Hz) power increase ratio during the visual stimulus that lasts for ~4 seconds.

B. Decoding ECoG High Gamma Power

In literature, it has been shown that the high gamma power in the extracellular recordings, such as local field potentials or ECoG, correlates with the firing activities of nearby neurons [16]. Consistently, as stated in the previous section, we also find increasing cellular activities in 2-photon calcium imaging accompanied with the high gamma power increases in ECoG recordings. Therefore, we investigate whether the ECoG high gamma power can be decoded using calcium fluorescence response from individual neurons. Spikes are obtained by deconvolution of calcium fluorescence, which is a good estimate for cellular spikes [11]. To do this, we first compute the ECoG high gamma power from one channel right above the ROI using the wavelet transform and down-sample the power trace to ~29 Hz to match the frame rate of the calcium

imaging. Note that, even though the high gamma band signal has a frequency higher than 29 Hz, its power change is much slower than 29 Hz. Therefore, this down-sampling operation does not cause any information loss or distortion of the high gamma power traces.

As shown in Figure 4, we use a 2-layer stacked LSTM recurrent neural network to decode the ECoG high gamma power from the cellular calcium activities of individual neurons from Layer II/III in the ROI. The first layer has 128 hidden units, while the second layer has 32 hidden units. We also apply 0.2 dropout after each LSTM layer to prevent overfitting. The network takes the deconvolved spikes of all the neurons (usually ~500 to ~700 neurons in one ROI) as input X_t. The time step of the network is set to 10. In order to make one prediction of the ECoG high gamma power at time t, the model considers the cellular spikes from the previous 9 time steps as well as the current time step. Then, the output of the 2nd LSTM layer is fed into the final output layer consisting of one output neuron with a linear activation function for continuous ECoG high gamma power decoding. In both awake and anesthetized states, the recordings last for ~37 minutes, amounting to ~62,000 samples. The first 30 minutes recordings are treated as the training data, whereas the last 7 minutes recordings are used as the test data to evaluate the decoding performance of the model.

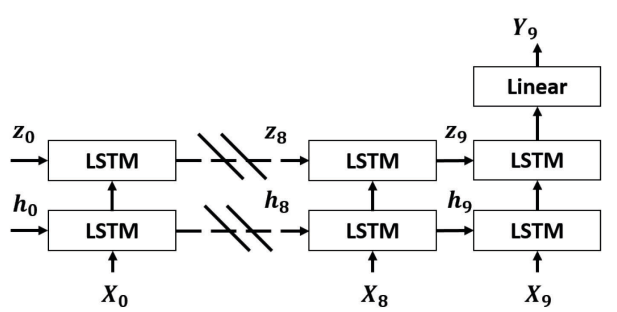


Figure 4. A diagram showing the 2-layer stacked LSTM network model used for the ECoG high gamma power decoding. X_t is the input vector at time step t that consists of the spiking activities from 500-700 individual neurons. h_t is the hidden state for the first layer LSTM and z_t is the hidden state for the second layer LSTM. Y_t is the decoded ECoG power at time step t.

In Figure 5a, the blue line shows the representative decoding result of the normalized ECoG high gamma power and the orange line stands for the true normalized ECoG high gamma power under anesthesia. It can be seen that most of the time, the model successfully decodes the stimulus related high gamma power increase (see the time segments labeled by the red bars). Besides that, during the absence of the visual stimulus, the model also predicts well the fluctuations of the high gamma power modulated by the 1-2Hz slow oscillations. Figure 5b shows the representative decoded and true normalized ECoG high gamma power traces under the awake state. In general, the model successfully decodes the high gamma power traces during both the stimulus-on and stimulus-off times. Note that under the awake state, the brain network is much less synchronized as opposed to the anesthetized case. Therefore, there is no slow oscillation modulated fluctuations which synchronizes large areas of the brain networks.

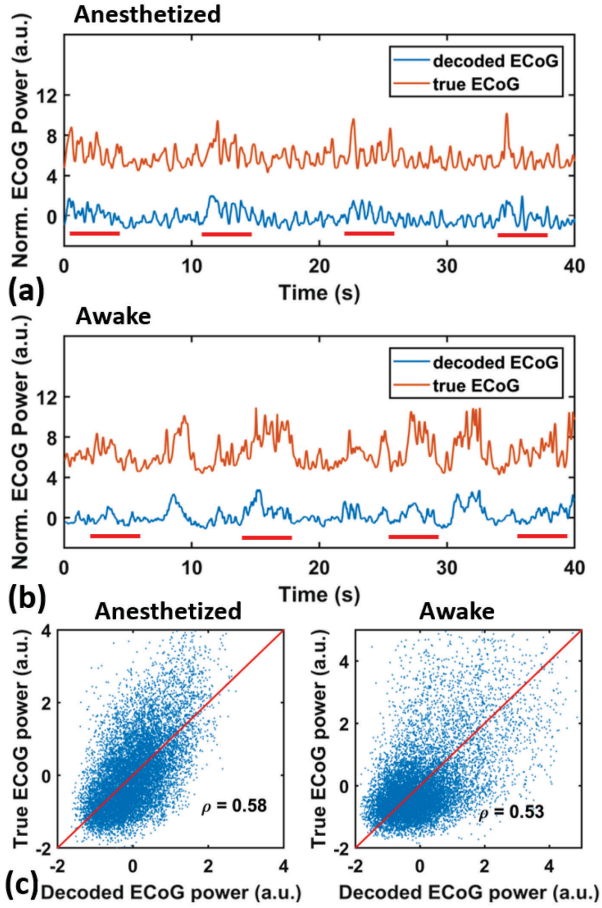


Figure 5. The decoding of ECoG high gamma power from one recording channel using the spiking activities from individual neurons. (a) Under anesthesia, the decoded normalized ECoG power follows closely with the true normalized ECoG power traces. It predicts both the visual stimulus related high gamma power elevation (the red bar segments) and power fluctuations modulated by the slow oscillations. (b) Under the awake state, the model predicts well in both the stimulus related time segments and the spontaneous activities when the stimulus is off. (c) The scatter plot of the target normalized ECoG power and the decoded values, showing high correlation, which indicates good similarity between the decoded and true ECoG power.

To examine the decoding quality of the model, in Figure 5c, we plot scatter plots to compare all the decoding/ground truth pairs at every test sample point (~12,000 points in total). For the awake state, the correlation between the decoded and true value is 0.53, which is similar to the 0.58 for anesthetized state. The decoding variance for awake state is slightly higher than that of the anesthetized state. This is because during the awake state, the neurons are more active and desynchronized than they are during anesthesia, leading to a larger variance in the ECoG high gamma power. Under the anesthetized state, the activities from a large brain network are more synchronized and correlated. Therefore, the cellular activities from layer II/III become more representative of the neural

activities in other areas. In summary, our model can make low variance decoding of the normalized ECoG high gamma power using cellular activities from neurons located at layer II/III for both anesthetized and awake states.

IV. CONCLUSION

In this work, we performed chronic multimodal studies in transgenic mouse models to record cellular calcium fluorescence response and cortical potentials simultaneously. We demonstrated stable chronic recordings for both electrophysiology and 2-photon calcium imaging over 20 days. We developed an LSTM recurrent neural network model for decoding ECoG high gamma power from the cellular calcium activities in layer II/III. Our model successfully decodes ECoG high gamma power under both awake and anesthetized states during and without stimulus. This work can pave the way towards linking findings from clinical human studies obtained by electrophysiology to discoveries enabled by high-resolution 2-photon microscopy in animal models.

REFERENCES

- L. Muller, G. Piantoni, D. Koller, S. S. Cash, E. Halgren, and T. J. Sejnowski, "Rotating waves during human sleep spindles organize global patterns of activity that repeat precisely through the night," *Elife*, vol. 5, p. e17267, 2016.
- [2] T. Yanagisawa et al., "Electrocorticographic control of a prosthetic arm in paralyzed patients
- " Annals of neurology, vol. 71, no. 3, pp. 353-361, 2012.
- [3] E. C. Leuthardt, G. Schalk, J. R. Wolpaw, J. G. Ojemann, and D. W. Moran, "A brain-computer interface using electrocorticographic signals in humans," *Journal of neural engineering*, vol. 1, no. 2, p. 63, 2004.
- [4] W. Wang *et al.*, "An electrocorticographic brain interface in an individual with tetraplegia," *PloS one*, vol. 8, no. 2, p. e55344, 2013.
- [5] O. G. Sani, Y. Yang, M. B. Lee, H. E. Dawes, E. F. Chang, and M. M. Shanechi, "Mood variations decoded from multi-site intracranial human brain activity," *Nature Biotechnology*, 2018.
- [6] H. Makino et al., "Transformation of Cortex-wide Emergent Properties during Motor Learning," *Neuron*, vol. 94, no. 4, pp. 880-890 e8, May 17 2017.
- [7] A. J. Peters, J. Lee, N. G. Hedrick, K. O'Neil, and T. Komiyama, "Reorganization of corticospinal output during motor learning," *Nature neuroscience*, vol. 20, no. 8, p. 1133, 2017.
- [8] M. Thunemann et al., "Deep 2-photon imaging and artifact-free optogenetics through transparent graphene microelectrode arrays," Nature communications, vol. 9, no. 1, p. 2035, 2018.
- [9] Y. Lu et al., "Ultralow Impedance Graphene Microelectrodes with High Optical Transparency for Simultaneous Deep Two - Photon Imaging in Transgenic Mice," Advanced Functional Materials, p. 1800002, 2018.
- [10] M. Pachitariu et al., "Suite2p: beyond 10,000 neurons with standard two-photon microscopy," Biorxiv, p. 061507, 2016.
- [11] M. Pachitariu, C. Stringer, and K. D. Harris, "Robustness of spike deconvolution for neuronal calcium imaging," *Journal of Neuroscience*, pp. 3339-17, 2018.
- [12] P. Lakatos, G. Karmos, A. D. Mehta, I. Ulbert, and C. E. Schroeder, "Entrainment of neuronal oscillations as a mechanism of attentional selection," *Science*, vol. 320, no. 5872, pp. 110-113, 2008.
- [13] M. Valencia, J. Artieda, J. P. Bolam, and J. Mena-Segovia, "Dynamic interaction of spindles and gamma activity during cortical slow oscillations and its modulation by subcortical afferents," *PloS one*, vol. 8, no. 7, p. e67540, 2013.
- [14] S. Ray and J. H. Maunsell, "Different origins of gamma rhythm and high-gamma activity in macaque visual cortex," *PLoS Biol*, vol. 9, no. 4, p. e1000610, Apr 2011.
- [15] G. Buzsáki and A. Draguhn, "Neuronal oscillations in cortical networks," *Science*, vol. 304, no. 5679, pp. 1926-1929, 2004.
- [16] G. Buzsaki and X. J. Wang, "Mechanisms of gamma oscillations," Annu Rev Neurosci, vol. 35, pp. 203-25, 2012.